New Phytologist

Research

Dry inside: progressive unsaturation within leaves with increasing vapour pressure deficit affects estimation of key leaf gas exchange parameters

Haoyu Diao[1], Lucas A. Cernusak[2], Matthias Saurer[1], Arthur Gessler[1,3], Rolf T. W. Siegwolf[1] and Marco M. Lehmann[1]

[1]Swiss Federal Institute for Forest, Snow and Landscape Research WSL, Birmensdorf, 8903, Switzerland; [2]College of Science and Engineering, James Cook University, Cairns, Qld, 4878, Australia; [3]Institute of Terrestrial Ecosystems, ETH Zurich, Zurich, 8092, Switzerland

Authors for correspondence:
Haoyu Diao
Email: haoyu.diao@wsl.ch

Marco M. Lehmann
Email: marco.lehmann@wsl.ch

Received: *8 June 2024*
Accepted: *8 August 2024*

New Phytologist (2024) **244:** 1275–1287
doi: 10.1111/nph.20078

Key words: carbon isotope, chloroplast, oxygen isotope, relative humidity, temperature.

Summary

- Climate change not only leads to higher air temperatures but also increases the vapour pressure deficit (VPD) of the air. Understanding the direct effect of VPD on leaf gas exchange is crucial for precise modelling of stomatal functioning.
- We conducted combined leaf gas exchange and online isotope discrimination measurements on four common European tree species across a VPD range of 0.8–3.6 kPa, while maintaining constant temperatures without soil water limitation. In addition to applying the standard assumption of saturated vapour pressure inside leaves (e_i), we inferred e_i from oxygen isotope discrimination of CO_2 and water vapour.
- e_i desaturated progressively with increasing VPD, consistently across species, resulting in an intercellular relative humidity as low as 0.73 ± 0.11 at the highest tested VPD. Assuming saturation of e_i overestimated the extent of reductions in stomatal conductance and CO_2 mole fraction inside leaves in response to increasing VPD compared with calculations that accounted for unsaturation. In addition, a significant decrease in mesophyll conductance with increasing VPD only occurred when the unsaturation of e_i was considered.
- We suggest that the possibility of unsaturated e_i should not be overlooked in measurements related to leaf gas exchange and in stomatal models, especially at high VPD.

Introduction

Driven by the ongoing effects of global change, air vapour pressure deficit (VPD) has increased considerably over recent decades on a global scale and is projected to continue rising in the future (IPCC, 2021; Fang *et al.*, 2022). This increase in VPD, coupled with the rise in global temperature, is considered to have adverse impacts on plant functioning and physiological processes related to leaf gas exchange (Fu *et al.*, 2022; Novick *et al.*, 2024). Such impacts are regarded as important reasons for tree mortality and growth decline in forests (Yuan *et al.*, 2019; Trotsiuk *et al.*, 2021; McDowell *et al.*, 2022; Shekhar *et al.*, 2023).

Variations in VPD influence leaf gas exchange by modifying the humidity gradient from the leaf intercellular air spaces to the atmosphere and by directly driving the movements of guard cells (Peak & Mott, 2011; Buckley, 2019). Studies have frequently indicated that leaf net photosynthesis rate (A_n) and transpiration rate (E) exhibit a nonlinear response to increasing VPD, often increasing to reach a maximum before declining (Farquhar, 1978; Franks *et al.*, 1997; Oren *et al.*, 1999; Shirke & Pathre, 2004; Devi & Reddy, 2018). However, an almost equivalent number of studies have instead revealed monotonic responses of A_n and E, with A_n decreasing but E increasing with increasing VPD (Dai *et al.*, 1992; Maroco *et al.*, 1997; Yong *et al.*, 1997; Urban *et al.*, 2017). This discrepancy is often attributed to the isohydric and anisohydric behaviours of plants: in response to increasing atmospheric water demand, isohydric plants minimise water loss through transpiration by closing their stomata, while anisohydric plants allow large fluctuations in leaf water status (Hochberg *et al.*, 2018). Additionally, the different VPD-response patterns of A_n and E may be partly explained by the response of leaf gas exchange to temperature, which tends to covary with VPD in nature (Duursma *et al.*, 2014). Therefore, disentangling the direct impact of VPD on leaf gas exchange from that of air temperature is crucial for understanding the underlying mechanisms of how variations in VPD and thus atmospheric drought influence plant functioning in a changing environment (Grossiord *et al.*, 2020; Smith *et al.*, 2020; Schönbeck *et al.*, 2022).

Stomata play a key role in regulating leaf gas exchange, implying that a correct estimation of stomatal behaviour is crucial in models of atmosphere–biosphere carbon dioxide (CO_2) and water (H_2O) fluxes. The standard practice for estimating stomatal conductance (g_s), and furthermore the CO_2 mole fraction in the leaf intercellular air spaces (c_i), in leaf gas exchange

measurements relies on a longstanding assumption that the air in the intercellular air spaces is saturated with water vapour (Gaastra, 1959; Moss & Rawlins, 1963; von Caemmerer & Farquhar, 1981). In other words, under this assumption, the intercellular vapour pressure (e_i) is equal to the saturation vapour pressure (e_s) at a given leaf temperature (T_{leaf}). One of the reasons that this assumption is made is simply that e_i cannot be measured directly. Only when the intercellular relative humidity (RH) is approximated as $e_i/e_s = 1$ can g_s be calculated from E and the vapour pressure of the air surrounding the leaf (e_a), assuming that the boundary layer conductance (g_b) is known (Gaastra, 1959). With g_s known, c_i can be calculated from A_n, E and the CO_2 mole fraction of the air surrounding the leaf (c_a), considering the diffusional processes of CO_2 from the atmosphere to the intercellular air spaces (Moss & Rawlins, 1963; von Caemmerer & Farquhar, 1981). The saturation assumption gained support from studies that indirectly showed that e_i stays near saturation across a variety of conditions (Farquhar & Raschke, 1978; Jones & Higgs, 1980; Sharkey *et al.*, 1982; Cernusak *et al.*, 2019).

An increasing number of studies have, however, shown evidence of unsaturation, that is $e_i/e_s < 1$ (Jarvis & Slatyer, 1970; Ward & Bunce, 1986; Egorov & Karpushkin, 1988; Karpushkin, 1994; Canny & Huang, 2006; Holloway-Phillips *et al.*, 2019). This phenomenon is especially notable in a few studies where there was evidence of progressive unsaturation of e_i with increasing VPD (Cernusak *et al.*, 2018; Wong *et al.*, 2022). The approach recently developed by Cernusak *et al.* (2018) for calculating intercellular RH provides a useful tool to further test the unsaturation hypothesis. It is based on simultaneous assessments of leaf gas exchange and isotope discrimination. In brief, the approach requires measurements of CO_2 and H_2O fluxes into and out of a leaf gas exchange cuvette and their carbon (C) and oxygen (O) isotope compositions. During the diffusion of CO_2 from the leaf intercellular air spaces into the chloroplast of C_3 plants, the O atoms in CO_2 exchange with those in the leaf water. This is driven by the enzyme carbonic anhydrase and is thought to reach a complete exchange at the chloroplast surface (Gillon & Yakir, 2000). From the measurements, the oxygen isotopic composition ($\delta^{18}O$) of CO_2 at the sites of carbonic anhydrase activity ($\delta^{18}O_{ca}$) can be determined by considering $C^{18}OO$ fractionation during CO_2 diffusion from the leaf intercellular air spaces to the chloroplast surface (Cernusak *et al.*, 2004). The e_i is involved in this calculation, as it contributes to the determination of c_i. Additionally, the $\delta^{18}O$ of CO_2 in equilibrium with water at the evaporative site ($\delta^{18}O_{ce}$) can be independently estimated from the $\delta^{18}O$ of transpired water and the Craig–Gordon equation (Craig & Gordon, 1965), which is also dependent on e_i. Because the chloroplast surface is appressed against the cell walls of the intercellular air spaces in C_3 plants, the $\delta^{18}O$ of water at the chloroplast surface can be assumed to be very close to that at the evaporative sites (Farquhar *et al.*, 1993; Busch *et al.*, 2013). Thus, an essential assumption of this approach is that $\delta^{18}O_{ca} = \delta^{18}O_{ce}$; with this assumption, e_i can be allowed to vary iteratively to solve for the value that satisfies the condition $\delta^{18}O_{ca} = \delta^{18}O_{ce}$. If unsaturation of e_i occurs as a rule rather than an exception, this implies that the saturation assumption applied for the analysis of leaf gas exchange measurements can cause biased estimations of g_s and c_i, as well as any further inferences (e.g. photosynthetic capacity) based on the two. Despite existing reports of unsaturated e_i values, there are still discrepancies regarding the extent to which unsaturation can occur with increasing VPD and how much the saturation assumption biases estimations of g_s and c_i. Updating our knowledge on this phenomenon is crucial, as it would fundamentally challenge prevailing understandings of water relations and water transport mechanisms (Buckley & Sack, 2019).

Furthermore, mesophyll conductance (g_m) is considered an important factor constraining CO_2 diffusion inside the leaf (Cousins *et al.*, 2020; Evans, 2021; Stangl *et al.*, 2022). The VPD responses of g_m may be linked to membrane and cell wall permeability, as well as CO_2 transport through aquaporins in response to VPD (Evans, 2021; Márquez & Busch, 2024). By complementing gas exchange measurements with $^{13}CO_2$ discrimination ($\Delta^{13}C$) assessments, the total mesophyll conductance to CO_2 diffusing from the intercellular spaces into the chloroplast stroma (g_{m13}) can be estimated. In addition, the mesophyll conductance to CO_2 diffusing from the intercellular spaces to the chloroplast surface (g_{m18}) can be estimated and thus differentiated from g_{m13} through measurements of $C^{18}OO$ discrimination ($\Delta^{18}O$) (Barbour *et al.*, 2016; Holloway-Phillips *et al.*, 2019; Diao *et al.*, 2024). More importantly, calculations of g_m enable additional estimations of the CO_2 mole fractions at the chloroplast surface (c_{ca}) and inside chloroplast stroma (c_c). Only a few studies have involved investigations of the VPD response of g_m; some indicated that g_m declined significantly with increasing VPD (Bongi & Loreto, 1989; Loucos *et al.*, 2017; Holloway-Phillips *et al.*, 2019), while others did not (Warren, 2008; Perez-Martin *et al.*, 2009; Stangl *et al.*, 2019; Wong *et al.*, 2022). It is also unclear how c_{ca} and c_c respond to variations in VPD (Márquez *et al.*, 2023). Since the effects of assuming saturation of e_i (or not) on the estimations of g_s and c_i are carried over to the estimations of g_m, c_{ca} and c_c (Cernusak *et al.*, 2019), it is necessary to investigate how the VPD responses of these variables are affected by assuming or not assuming saturation. Studies targeting this knowledge gap will help us gain a better mechanistic understanding of the VPD response of leaf gas exchange.

In this study, we performed combined classical online leaf gas exchange measurements and online isotope discrimination assessments on potted saplings of four common European tree species (*Fagus sylvatica*, *Picea abies*, *Quercus petraea*, and *Tilia cordata*) under nonlimiting soil water supply. We carried out the measurements under finely controlled humidity and temperature conditions, spanning a VPD gradient of 0.8–3.6 kPa at both 30°C and 35°C (near optimum temperatures for photosynthesis), with two species assessed at each temperature. We aimed to: (1) investigate the direct VPD responses of leaf gas exchange and isotope discrimination at constant temperatures; (2) evaluate the direct effect of VPD on e_i; and (3) assess the direct VPD responses of g_s, g_m and leaf internal CO_2 mole fractions, considering two scenarios: one assuming a saturated e_i over the VPD gradient, and the other accounting for a progressive unsaturation of e_i at moderate to high VPD. Our findings suggest that future estimations of key leaf gas exchange parameters should account for unsaturation

inside the leaf as a real phenomenon, which facilitates more accurate modelling of plant physiological responses to environmental changes.

Materials and Methods

Plant material

Five 2-yr-old saplings of each *Fagus sylvatica* L., *Picea abies* (L.) H. Karst., *Quercus petraea* (Matt.) Liebl., and *Tilia cordata* Mill. were used in this study. The saplings were planted into 4 l pots with soil mixed with commercial slow-release NPK fertilizer (Osmocote Exact Standard 3–4 M; ICL, Suffolk, UK), then transferred to a climate chamber (Bitzer 6HE-35Y; Kälte 3000 AG, Landquart, Switzerland) to induce leaf flushing. The environmental conditions were air temperature of 25°C, RH of 60%, and light intensity of 110 µmol m^{-2} s^{-1} during a photoperiod of 18 h; during night-time the air temperature was 15°C and RH 50%. One month later, the plants were transferred to a glasshouse and grew under natural light conditions for 3 months. During this period, the average air temperature was 22.8°C, the average RH was 54.1% and the average air VPD was 1.3 kPa. Throughout the experiment, the plants were watered every 2 d, such that the trays beneath the pots always contained liquid water.

Instrumental setup and calibrations

Online stable isotope techniques, characterized by the combined instrumentation of a leaf gas exchange system (all components from Heinz Walz GmbH, Effeltrich, Germany) and CO_2 and H_2O isotope analysers (Delta Ray; Thermo Fisher Scientific Inc., Bremen, Germany and L2120-i; Picarro Inc., Santa Clara, CA, USA, respectively), were used to measure leaf gas exchange and isotope discrimination at the same time. The leaf gas exchange system included a portable photosynthesis control unit (GFS-3000), a leaf gas exchange cuvette (3010-GWK1) and a light source (RGBW-L084). The leaf cuvette was temperature and humidity controlled and supplied with a transversal fan mixing the air inside the cuvette, minimizing the leaf boundary layer resistance and ensuring homogeneous distributions of cuvette temperature (T_{cuv}), humidity and the CO_2 mole fraction inside the cuvette (c_a). T_{leaf} was measured inside the leaf cuvette using a thermocouple (3010-CA/TCL). A bypass humidity control system (NFRB0101) served as an additional measure to keep the humidity in the cuvette constant at the preselected value.

The gas exchange system was coupled to the CO_2 and H_2O isotope analysers. With an interposed multiport valve (VICI; Valco Instruments Co. Inc., Houston, TX, USA), and the air streams entering or leaving the leaf cuvette were selected alternately for isotope analysis. Carbon isotopic composition ($\delta^{13}C$) in CO_2 was expressed against Vienna Pee Dee Belemnite, and $\delta^{18}O$ in CO_2 and H_2O vapour were expressed against Vienna Standard Mean Ocean Water. The gas exchange system and the VICI valve were connected via an open split to prevent pressure surges caused by valve switching (Diao *et al.*, 2024).

The gas exchange system, the VICI valve and the plant being measured were placed in a climate chamber (Conviron PGR15; Controlled Environments Ltd, Winnipeg, MB, Canada), and the environmental conditions in the chamber were set to match those in the leaf cuvette. The tube connecting the VICI valve to the isotope analysers was heated to 65°C using a heating band (HTS System AG, Hünenberg, Switzerland). These instrumental arrangements prevented potential condensation inside the instrument system and kept the whole plant at similar environmental conditions. More details of the instrumental setup, with schematics and the operation and calibration procedures, can be found in Diao *et al.* (2024).

Measurement protocol

One day before the measurements, plants of a given species were transferred from the glasshouse to the climate chamber. During the measurements, one foliated branch (for *F. sylvatica* and *P. abies*) or one entire leaf (for *Q. petraea* and *T. cordata*) was placed in the cuvette. Note that the gas exchange system accepts input VPD values derived from T_{leaf} (i.e. leaf-to-air vapour pressure difference, LAVPD) in Pa kPa^{-1}. This unit needs to be corrected for atmospheric pressure (P_{atm}) to be converted to the unit of kPa. The LAVPD was increased from *c.* 1 to 4 kPa in steps of *c.* 1 kPa during the measurements. Afterwards, the air VPD was derived using the measured e_a inside the cuvette and e_s was calculated from the Goff–Gratch equation (Goff & Gratch, 1946) based on the T_{cuv}. This resulted in an ecologically meaningful air VPD gradient of 0.8–3.6 kPa in steps of *c.* 1 kPa (i.e. 0.79, 1.76, 2.69 and 3.63 kPa; Supporting Information Fig. S1). A VPD of 3.6 kPa is very close to the highest historical annual average VPD in the arid climate zone (3.4 kPa, 1981–2020), as derived from climate models (Fang *et al.*, 2022). Likewise, a mean daily daytime VPD *c.* 3.6 kPa was observed in temperate forest sites under extreme hot droughts (Shekhar *et al.*, 2023). Under this condition, stem cell expansion, and thus tree growth, may no longer be possible (Zweifel *et al.*, 2021; Novick *et al.*, 2024).

For each VPD step, the target T_{cuv} was 30°C for *Q. petraea* and *P. abies* and 35°C for *F. sylvatica* and *T. cordata*. For each species and VPD step, photosynthetically active radiation at the leaf surface was 800 µmol m^{-2} s^{-1} (light saturation) and c_a was 400 µmol mol^{-1}. When the gas exchange rates were at steady state (*c.* 40 min), the gas exchange and the isotope ratio data were recorded.

Calculations of intercellular RH from $\delta^{18}O$

The ratio e_i/e_s was resolved from the coupled measurements of $\Delta^{18}O$ and leaf gas exchange based on Cernusak *et al.* (2018) and Cernusak *et al.* (2019). In brief, the method requires measurements of $\delta^{18}O$ from both H_2O and CO_2. These measurements provide the necessary information to establish the constraint that the $\delta^{18}O$ of CO_2 at the sites of carbonic anhydrase activity matches that in equilibrium with evaporative site water, through which e_i/e_s can be resolved iteratively. A detailed description of the equations used to calculate e_i/e_s is provided in Method S1.

Meanwhile, we refer readers to the simplified algebraic flow path provided in Cernusak *et al.* (2018) and the spreadsheet available in Cernusak *et al.* (2019) as useful tools for understanding and implementing the methodology. A list of abbreviations and symbols used in this study is provided in Table 1.

In the iteration loop of e_i/e_s, an additional unknown parameter, g_{m18}, is involved. Because g_{m18} cannot be solved without knowing c_i beforehand and c_i is only estimated later from e_i/e_s (to be described later) without assuming saturation, it is necessary to use assumed g_{m18} values across the VPD steps. In this study, the lowest measured air VPD was maintained at 0.79 kPa, $e_i/e_s = 1$ could be assumed under this condition. Thus, for each tree which was measured at the lowest VPD, we iteratively varied g_{m18} until the value was found at which $\delta^{18}O_{ca} = \delta^{18}O_{ce}$ with a constraint of $e_i/e_s = 1$. The solved g_{m18} values at the lowest VPD were further assigned to the measurements of the respective tree at higher air VPD conditions. Note that after e_i/e_s values were estimated, e_i was further derived from e_s at T_{leaf} according to the temperature–e_s relationship of Goff & Gratch (1946). The data used in this study are provided in the Dataset S1.

Table 1 Definitions of symbols used repeatedly in the main text.

Symbol	Definition
A_n	Net photosynthesis rate
c_a	CO_2 mole fraction of the air surrounding the leaf
c_c	CO_2 mole fraction in the chloroplast stroma
c_{ca}	CO_2 mole fraction at the sites of carbonic anhydrase activity
c_i	CO_2 mole fraction in the leaf intercellular air spaces
$\Delta^{13}C$	Photosynthetic C isotope discrimination of CO_2
$\Delta^{13}C_{obs}$	Observed discrimination against $^{13}CO_2$ during photosynthesis
$\Delta^{18}O$	Photosynthetic O isotope discrimination of CO_2
$\Delta^{18}O_{obs}$	Observed discrimination against $C^{18}OO$ during photosynthesis
$\delta^{18}O_A$	$\delta^{18}O$ of CO_2 taken up by net photosynthesis
$\delta^{18}O_{ca}$	$\delta^{18}O$ of CO_2 at the sites of carbonic anhydrase activity
$\delta^{18}O_{ce}$	$\delta^{18}O$ of CO_2 in equilibrium with evaporative site water
$\delta^{18}O_e$	$\delta^{18}O$ of water at evaporative sites in leaves
$\delta^{18}O_E$	$\delta^{18}O$ of transpired water vapour
$\delta^{18}O_i$	$\delta^{18}O$ of CO_2 in the intercellular air spaces
E	Transpiration rate
e_a	Vapour pressure of the air surrounding the leaf
e_i	Vapour pressure in the leaf intercellular air spaces
e_s	Vapour pressure at saturation, calculated as a function of temperature
g_b	Leaf boundary layer conductance to water vapour
g_m	Mesophyll conductance to CO_2
g_{m13}	Mesophyll conductance to CO_2 estimated from ^{13}C measurements, representing the mesophyll conductance from leaf intercellular air spaces to sites of carboxylation (i.e. total mesophyll conductance)
g_{m18}	Mesophyll conductance to CO_2 estimated from ^{18}O measurements, representing the mesophyll conductance from leaf intercellular air spaces to sites of carbonic anhydrase (i.e. cell wall and plasma membrane conductance)
g_s	Stomatal conductance to water vapour
g_t	Conductance to water vapour from leaf intercellular air spaces to the atmosphere
g_{tc}	Conductance to CO_2 from leaf intercellular air spaces to the atmosphere
RH	Relative humidity
T_{cuv}	Cuvette temperature
T_{leaf}	Leaf temperature
VPD	Air vapour pressure deficit

Symbols that appear only alongside their definition in the text are not included here.

Calculations of stomatal conductance and intercellular CO_2 mole fraction with and without assumed saturation

A_n and E values were calculated by the Walz GFS-3000 gas exchange system, according to von Caemmerer & Farquhar (1981). For each individual measurement, g_s and c_i were calculated using an identical set of equations and either substituting e_i with e_s ($e_i/e_s = 1$) to refer to the saturation assumption at VPD of 0.8 kPa or using e_i independently derived from the $\Delta^{18}O$ measurements to account for unsaturation at VPD > 0.8 kPa as follows (von Caemmerer & Farquhar, 1981).

The variable g_s was given as:

$$g_s = \frac{1}{\frac{1}{g_t} - \frac{1}{g_b}} \quad \text{Eqn 1}$$

where g_t is the total conductance to water vapour from leaf intercellular air spaces to the atmosphere, and g_b is assumed to be 3.5 mol H_2O m^{-2} s^{-1} for the chamber and fan speed used in our measurements (Cernusak *et al.*, 2019; Diao *et al.*, 2024).

The variable g_t was given as:

$$g_t = \frac{E \times \left(1 - \frac{e_i + e_a}{2P_{atm}}\right)}{\frac{e_i - e_a}{P_{atm}}} \quad \text{Eqn 2}$$

The variable c_i was given as:

$$c_i = \frac{\left(g_{tc} - \frac{E}{2}\right) \times c_a - A_n}{g_{tc} + \frac{E}{2}} \quad \text{Eqn 3}$$

where g_{tc} is the total conductance to CO_2, expressed as $1/(1.6/g_s + 1.37/g_b)$.

Calculations of chloroplastic CO_2 mole fraction and mesophyll conductance

The CO_2 mole fraction at the chloroplast surface (c_{ca}), the assumed site of carbonic anhydrase activity, can be derived from $\delta^{18}O$ measurements according to Barbour *et al.* (2016).

$$c_{ca} = c_i \left(\frac{\delta^{18}O_i - \bar{a} - \alpha_{ac}\delta^{18}O_A}{\delta^{18}O_{ce} - \bar{a} - \alpha_{ac}\delta^{18}O_A} \right) \quad \text{Eqn 4}$$

where α_{ac} is the $^{18}O/^{16}O$ fractionation factor for CO_2 diffusing across the boundary layer and stomata, defined as $1+\bar{a}$. The variable $\bar{a}$ was calculated as described in Diao *et al.* (2024). Here, c_i was derived by employing the saturation assumption across the VPD steps; Eqn 4 was, therefore, used to calculate c_{ca} assuming saturation of e_i.

In the calculations associated with unsaturation, c_i cannot be derived from the iteration if c_{ca} is not known first. Therefore, the c_{ca} which accounted for unsaturation of e_i was calculated (Eqn 5) by

assuming that the g_{m18} values determined at the lowest VPD step for each leaf remained unchanged at the other VPD steps and by using the c_i for which unsaturation was taken into account (Eqn 3).

$$c_{ca} = c_i - \frac{A_n}{g_{m18}} \quad \text{Eqn 5}$$

The variable g_{m13} was expressed as:

$$g_{m13} = \frac{1+t}{1-t}\left(\frac{b - a_m - \frac{\alpha_b}{\alpha_e \alpha_R} e' \frac{\mathscr{R}_{day}}{A_n}}{\Delta^{13}C_i - \Delta^{13}C_{obs}}\right)\frac{A_n}{c_a} \quad \text{Eqn 6}$$

where a_m is the $^{13}C/^{12}C$ fractionation for CO_2 dissolution and diffusion from the intercellular air spaces to the sites of carboxylation in the chloroplasts (1.8‰), and b is the $^{13}C/^{12}C$ fractionation associated with carboxylation (30‰). $e' = e + e^*$, where e is the $^{13}C/^{12}C$ fractionation during day respiration (−3‰) and e^* is an additional apparent fractionation accounting for the difference in substrate composition between freshly assimilated C and old C pools (Wingate *et al.*, 2007). e^* was assumed to be zero in our case (Diao *et al.*, 2024). α_b and α_e are defined as $1 + b$ and $1 + e$, respectively. R_{day} is the day respiration rate and assumed to be half of the dark respiration rate (R_{dark}) (Adnew *et al.*, 2020). The R_{dark} measurements were described in Diao *et al.* (2024). $\alpha_R = 1 + (R_{day}/A_n)(e/\alpha_e)$ (Busch *et al.*, 2020). The ternary correction term, t, was calculated according to Farquhar & Cernusak (2012). $\Delta^{13}C_{obs}$ is the observed discrimination against ^{13}C during CO_2 assimilation, which was calculated following Evans *et al.* (1986). $\Delta^{13}C_i$ is the modelled C isotope discrimination, which was calculated according to Busch *et al.* (2020). Detailed descriptions of the calculations are presented in Diao *et al.* (2024). Note that the c_i values calculated both with the saturation assumption and with the unsaturation of e_i accounted for were used in the calculations of g_{m13} for comparison.

The CO_2 mole fraction inside the chloroplast stroma (c_c) was then calculated separately for the saturation and unsaturation cases, as:

$$c_c = c_i - \frac{A_n}{g_{m13}} \quad \text{Eqn 7}$$

Statistical analysis

All statistical analyses were conducted using R software v.4.3.1 (R Core Team, 2023). The responses of the studied variables to air VPD were analysed using linear mixed models with the IMERTEST package in R (Kuznetsova *et al.*, 2017), with air VPD as a fixed effect and both species and T_{cuv} groups (i.e. $T_{cuv} = 30°C$ and 35°C) as random effects. Because the T_{cuv} groups were treated as random effects in our statistical analyses, and we did not observe apparent separation of the VPD-response curves based on T_{cuv} in our dataset, we confidently conclude that temperature-specific patterns were not evident in this study and that the observed physiological responses were purely driven by VPD. The between-group sum of squares of an analysis of variance (ANOVA) was used to compare the differences in interspecies variabilities between g_s calculated with and without assuming saturation of e_i. Two-sample t-tests were performed to test the significance of differences in g_s and g_{m13} when assuming saturation of e_i and when accounting for unsaturation of e_i. For $\Delta^{13}C_{obs}$ and the observed discrimination against ^{18}O during CO_2 assimilation ($\Delta^{18}O_{obs}$), a filter ($\xi < 30$, defined in Eqn S6) was applied to exclude data with low confidence in the isotopic discrimination estimates (Diao *et al.*, 2024).

Results

Experimental conditions

T_{cuv} was kept constant along the VPD gradient, with a mean value (±1 SD) of 30.0 ± 0.0°C for *P. abies* and *Q. petraea*, and of 35.0 ± 0.0°C for *F. sylvatica* and *T. cordata* (Fig. S1). T_{leaf} was slightly higher than T_{cuv}, with a mean value of 30.3 ± 0.1°C for *P. abies* and *Q. petraea*, and of 35.2 ± 0.1°C for *F. sylvatica* and *T. cordata*. For these two groups of T_{cuv}, VPD was increased stepwise from 0.8 ± 0.1 to 3.6 ± 0.1 kPa, resulting in decreases in RH from 78.3% ± 2.8% to 13.4% ± 2.0% and from 78.5% ± 1.1% to 32.2% ± 1.3%, respectively. These relationships match well with the theoretical relationship between VPD and RH at constant temperatures (Fig. S1), suggesting precise temperature and humidity control in the gas exchange system.

Responses of A_n, E, and C and O isotope discriminations to increasing VPD

The directions of responses of A_n and E to increasing air VPD were consistent among the four studied species (Fig. 1). Based on the analyses of linear mixed models and averaged across the species, A_n decreased significantly from 5.4 ± 1.6 to 3.9 ± 1.1 μmol CO_2 m^{-2} s^{-1} with increasing air VPD (Fig. 1a; $F = 17.51$, $P < 0.001$), whereas E increased significantly from 1.2 ± 0.4 to 1.8 ± 0.8 mmol H_2O m^{-2} s^{-1} with increasing air VPD (Fig. 1b; $F = 16.19$, $P < 0.001$). Note that the VPD response of A_n was much less pronounced for *F. sylvatica* than for the other three species, with a slope of −0.22 μmol CO_2 m^{-2} s^{-1} kPa^{-1} for *F. sylvatica* and a slope of −0.71 μmol CO_2 m^{-2} s^{-1} kPa^{-1} averaged across the remaining species (Fig. 1a).

We found significant responses of $\Delta^{13}C_{obs}$ ($F = 7.81$, $P = 0.007$) and $\Delta^{18}O_{obs}$ ($F = 23.73$, $P < 0.001$) to increasing air VPD across the species (Fig. S2). On average, $\Delta^{13}C_{obs}$ decreased with increasing air VPD, from 19.7 ± 1.9 to 17.3 ± 2.1‰ (Fig. S2a), while $\Delta^{18}O_{obs}$ increased from 35.0 ± 10.4 to 45.9 ± 11.3‰ (Fig. S2b). However, for *F. sylvatica*, the linear relationship between $\Delta^{13}C_{obs}$ and air VPD was not statistically significant (Fig. S2a; $P = 0.98$).

Responses of RH inside the leaf to VPD

We constrained the values of the leaf intercellular RH as $e_i/e_s = 1$ at the lowest measured VPD (< 1 kPa), ensuring that these values explicitly align with the assumption that the air inside the leaf is

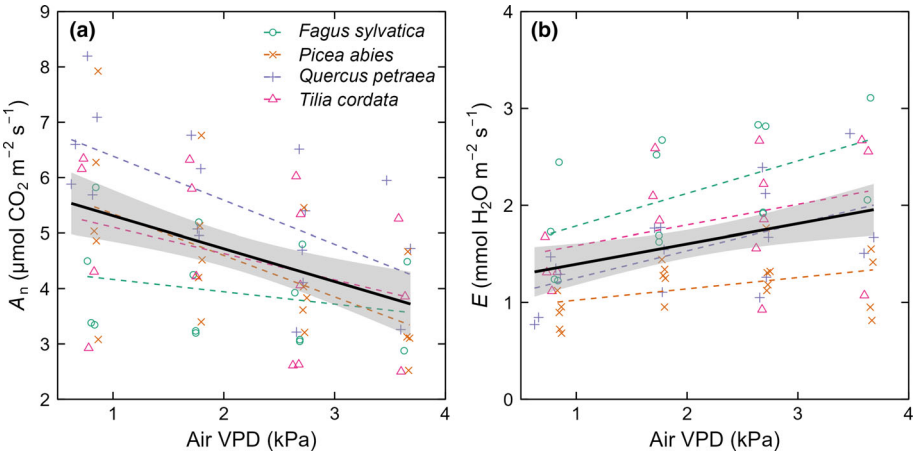

Fig. 1 Responses of (a) net photosynthesis rate (A_n) and (b) transpiration rate (E) to increasing air vapour pressure deficit (VPD) in four tree species. Each dashed line represents the linear trend for one tree species. The solid line and the grey band represent the linear trend averaged across all tree species and its 95% confidence interval, respectively. Different symbols and colours indicate different tree species ($n = 5$ per VPD step).

saturated with water vapour under low VPD (Fig. 2). At VPD > 1 kPa, intercellular RH was calculated from the $\delta^{18}O$ measurements (see Materials and Methods section). This approach takes unsaturation of e_i into account. Across the species, intercellular RH decreased significantly with increasing air VPD ($F = 91.83$, $P < 0.001$), suggesting a progressive unsaturation inside the leaf. Specifically, across the species which were measured at 30°C and 35°C, a linear regression showed that with every 1 kPa increase in air VPD, intercellular RH decreased by 0.10 ± 0.01 (slope ± SE for the regression model). At the highest measured VPD (i.e. 3.6 ± 0.1 kPa), the intercellular RH was 0.73 ± 0.11.

VPD responses of g_s and g_m with and without assuming saturation of e_i

The g_s showed a consistent pattern of decrease with increasing VPD, both with and without the saturation assumption (Fig. 3). Across all species, a reciprocal function fit the responses well ($P < 0.001$ and $P = 0.01$ under saturation assumed and unsaturation accounted for, respectively), and the decreases were statistically significant when both species and T_{cuv} groups were included in the models as random effects ($F = 91.92$ and 9.02, respectively; $P < 0.01$ for both). However, the VPD-response pattern of the g_s calculated with the saturation assumption (Fig. 3a) was more distinct than that calculated accounting for unsaturation (Fig. 3b). The difference in average g_s between the lowest and highest VPD was much smaller (0.05 mol H_2O m^{-2} s^{-1}) and the inter-species variability of the values was much higher (0.06; between-species sum of squares, ANOVA) for the case accounting for unsaturation (Fig. 3b), than when saturation was assumed (0.09 mol H_2O m^{-2} s^{-1}, 0.03; Fig. 3a). Moreover, for VPD > 0.8 kPa, the g_s calculated accounting for unsaturation (Fig. 3b) was significantly higher (0.03 mol H_2O m^{-2} s^{-1}; $P < 0.001$, t-test) than the g_s when saturation was assumed (Fig. 3a).

No significant response of g_{m13} to increasing air VPD was found when saturation of e_i was assumed, although the smoothed trend indicated somewhat higher g_{m13} values on average when VPD was also high (Fig. 4a). By contrast, when unsaturation was accounted for, g_{m13} decreased significantly with increasing VPD across the species ($F = 6.95$, $P = 0.01$), ranging from 0.10 ± 0.06 mol CO_2 m^{-2} s^{-1} at the lowest measured VPD to 0.06 ± 0.03 mol CO_2 m^{-2} s^{-1} at the highest measured VPD (Fig. 4b). However, for *F. sylvatica*, the linear relationship between g_{m13} and air VPD was not statistically significant (Fig. 4b; $P = 0.90$).

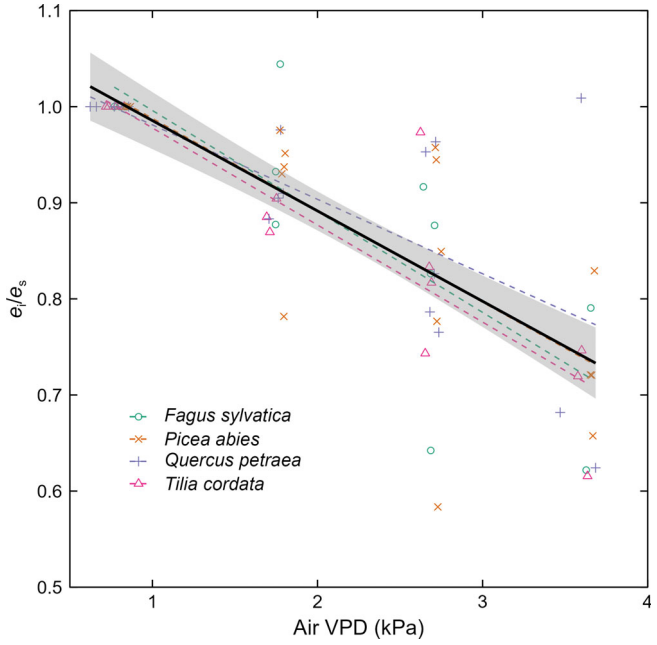

Fig. 2 Response of leaf intercellular relative humidity (e_i/e_s) to increasing air vapour pressure deficit (VPD) in four tree species. The e_i/e_s values were estimated from measurements of oxygen isotope discrimination in CO_2 and transpired water vapour. At the lowest VPD step, $e_i/e_s = 1$ was applied to meet the assumption of vapour saturation inside the leaf. Each dashed line represents the linear trend for one tree species. The solid line and the grey band represent the linear trend averaged across all tree species and its 95% confidence interval, respectively. Different symbols and colours indicate different tree species ($n = 5$ per VPD step).

Responses of the CO_2 mole fraction inside the leaf to VPD with and without assuming saturation of e_i

Across the air VPD gradient, the average CO_2 mole fractions within leaves decreased progressively from the outside

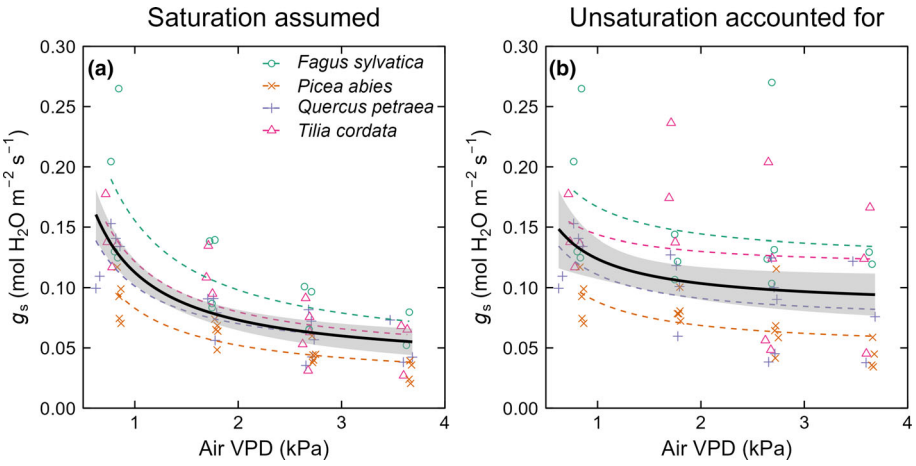

Fig. 3 Responses of stomatal conductance (g_s) to increasing air vapour pressure deficit (VPD) in four tree species. Saturation of the leaf intercellular vapour pressure (e_i) was assumed in calculations for the g_s values in (a), whereas unsaturation was taken into account in calculations for the g_s values in (b). Each dashed line represents the regression of a reciprocal function ($y = 1/x$) for one species. Different symbols and colours indicate different tree species ($n = 5$ per VPD step). The solid line and the grey band represent the regression of a reciprocal function ($y = 1/x$) averaged across all tree species and its 95% confidence interval, respectively.

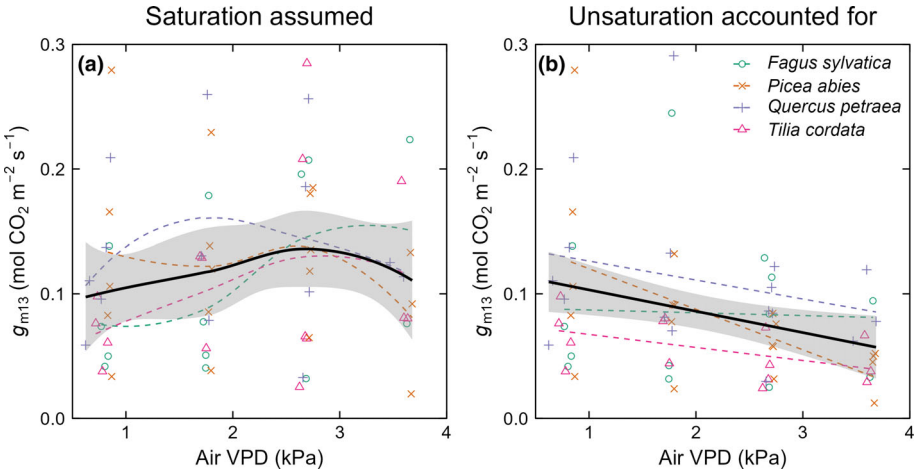

Fig. 4 Responses of mesophyll conductance to CO_2 estimated from ^{13}C measurements (g_{m13}) to increasing air vapour pressure deficit (VPD) in four tree species. Saturation of the leaf intercellular vapour pressure (e_i) was assumed in calculations for the g_{m13} values in (a), whereas unsaturation was taken into account in calculations for the g_{m13} values in (b). In (a), each dashed line represents a local polynomial regression fitting for one tree species. The solid line and the grey band represent a local polynomial regression fitting averaged across all species and its 95% confidence interval, respectively. In (b), each dashed line represents the linear trend for one species. The solid line and the grey band represent the linear trend averaged across all species and its 95% confidence interval, respectively. In both panels, different symbols and colours indicate different tree species ($n = 5$ per VPD step).

in: $c_i/c_a > c_{ca}/c_a > c_c/c_a$ (Fig. 5). This pattern held both with and without the saturation assumption (both $P < 0.001$). With the saturation assumption, c_i/c_a ($F = 137.07$, $P < 0.001$), c_{ca}/c_a ($F = 11.51$, $P = 0.001$), and c_c/c_a ($F = 24.02$, $P < 0.001$) decreased significantly with increasing air VPD (Fig. 5a–c), but the decreasing trend in c_{ca}/c_a (Fig. 5b) was not as substantial as that of c_i/c_a and c_c/c_a (Fig. 5a, c). Accounting for unsaturation, c_i/c_a ($F = 10.67$, $P = 0.002$) and c_c/c_a ($F = 14.47$, $P < 0.001$) decreased significantly with the increase in air VPD, but this was not found for c_{ca}/c_a ($F = 3.46$, $P = 0.07$) (Fig. 5d–f).

Regarding the rates of changes in the CO_2 mole fractions with increasing air VPD, c_i/c_a decreased less with increasing VPD when unsaturation was taken into account than when saturation was assumed, as shown by the different slopes of the linear fittings (−0.02, Fig. 5d vs −0.08, Fig. 5a). For c_{ca}/c_a and c_c/c_a, the decreasing rates were not distinctly different when saturation was assumed (Fig. 5b,c) or not (Fig. 5e,f).

Discussion

Progressive unsaturation of e_i with increasing VPD

We quantitatively estimated e_i/e_s values of the four studied tree species as they were exposed to increasing VPD, using measurements of $\delta^{18}O$ of CO_2 and water vapour (Cernusak *et al.*, 2018). We found strong signals of unsaturation and the degree of unsaturation increased linearly with the increase in VPD (Fig. 2). In agreement with the evidence of unsaturation shown in this study, Cernusak *et al.* (2018) reported that intercellular RH declined to values in the range of 0.9 in *Pinus edulis* at *c.* 5 kPa VPD and 0.8 in *Juniperus monosperma* at *c.*

New Phytologist

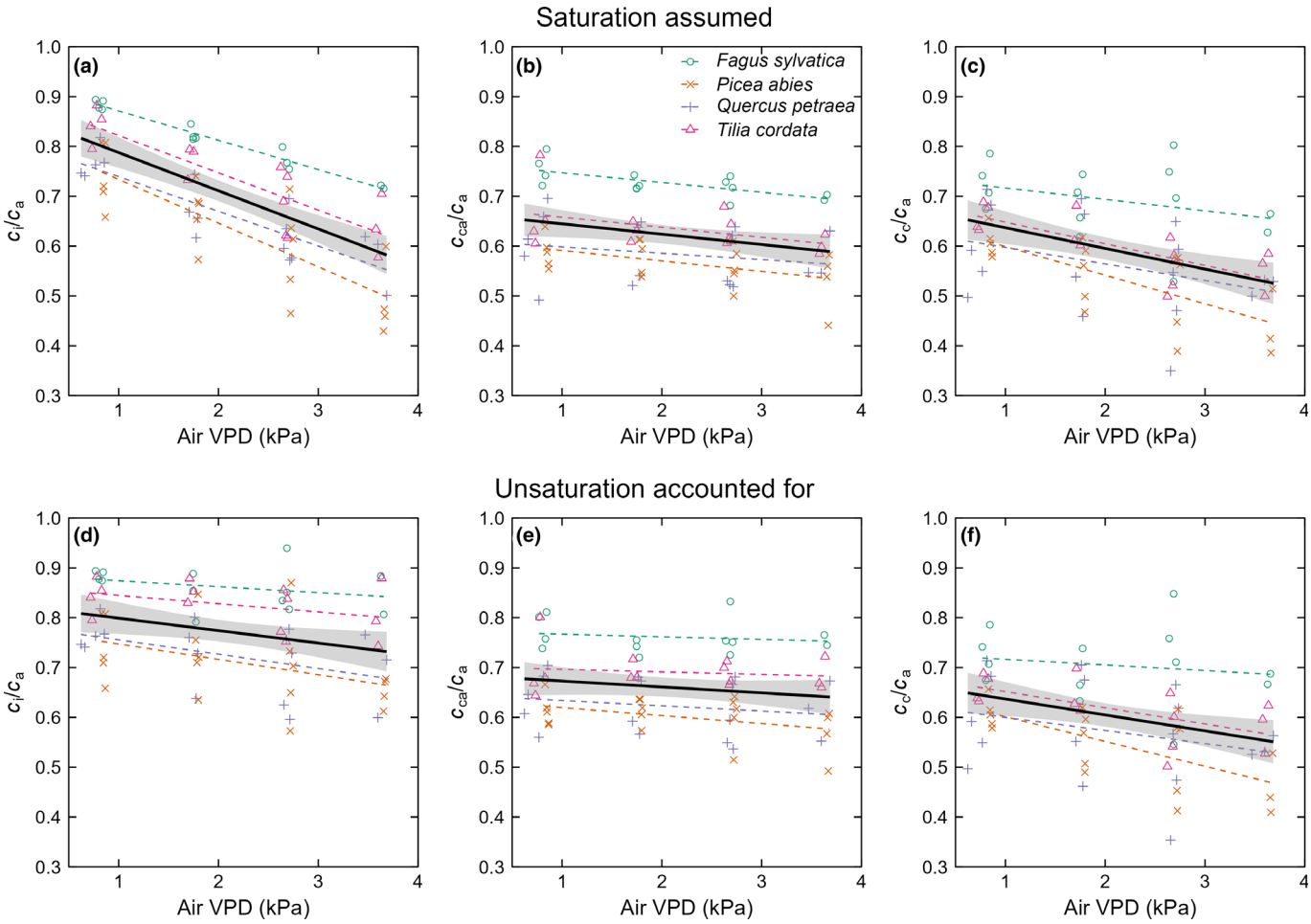

Fig. 5 Air vapour pressure deficit (VPD) responses of the ratio of intercellular to ambient CO_2 mole fraction (c_i/c_a; a, d); the ratio of chloroplast surface to ambient CO_2 mole fraction (c_{ca}/c_a; b, e); and the ratio of chloroplast stroma to ambient CO_2 mole fraction (c_c/c_a; c, f). Unsaturation of the leaf intercellular vapour pressure (e_i) was taken into account in calculations for (d–f) but not for (a–c). Each dashed line represents the linear trend for one species. Different symbols and colours indicate different tree species ($n = 5$ per VPD step). The solid line and the grey band represent the linear trend averaged across all species and its 95% confidence interval, respectively.

4 kPa VPD; Holloway-Phillips *et al.* (2019) reported that intercellular RH declined to *c.* 0.95 in *Vicia faba* at *c.* 2 kPa VPD; and Wong *et al.* (2022) reported that intercellular RH decreased to 0.8 in *Gossypium hirsutum* and to 0.9 in *Helianthus annuus* at *c.* 2 kPa VPD. The extent of the decrease in intercellular RH as VPD rises in our study (i.e. decrease of 0.1 per 1 kPa increase in VPD) shows close agreement with the values reported by Holloway-Phillips *et al.* (2019) and Wong *et al.* (2022). Even though this decline is more severe than what was reported by Cernusak *et al.* (2018), it is still lower than the slope of 0.23 kPa^{-1} found in the transgenic *Populus* × *canescens* transformed with the *Arabidopsis thaliana* mutant *abi1* gene, which has a defective stomatal closure response to VPD, therefore, reflecting an extreme case of unsaturation (Cernusak *et al.*, 2019). In addition, the results of the studies mentioned above and this study together suggest that the saturation assumption is generally reliable for leaf gas exchange measurements at VPD < 1 kPa. Still, further studies on direct observations of stomata are required to assess the degree of unsaturation across a range of VPD in different species acclimatised to diverse environmental conditions.

The reliability of the method we used to estimate e_i was critically evaluated in Cernusak *et al.* (2018). They concluded that a decline in e_i below saturation as VPD increased is the most likely explanation for the progressively higher $\delta^{18}O_i$ values compared with $\delta^{18}O_{ce}$, suggesting the robustness of the method in capturing potential unsaturation of e_i. In addition, as acknowledged in Cernusak *et al.* (2018), the method we used to estimate e_i is sensitive to the choice of g_{m18} values. Recently, Holloway-Phillips *et al.* (2019) developed a two-source $\delta^{18}O$ method, which does not need assumed g_{m18} values to estimate e_i; they found a decrease in g_{m18} with increasing air VPD ($g_{m18} = -0.13VPD + 0.97$). We further performed a sensitivity analysis with g_{m18} values that decrease with increasing VPD, based on the observations in Holloway-Phillips *et al.* (2019) (see Supporting Information). We found that the e_i calculated with VPD-sensitive g_{m18} values generally decreased more strongly with increasing VPD than in the case of constant g_{m18} (Fig. S3).

Moreover, an essential assumption of the oxygen isotope method is that $\delta^{18}O_{ca} = \delta^{18}O_{ce}$, which implies that carbonic anhydrase activity is sufficiently high to drive full equilibration between CO_2 and water at the evaporative sites across the VPD gradient. By contrast, the c_i difference technique developed by Wong *et al.* (2022) does not require this assumption. The comparison, illustrated in Extended Data fig. 2 of Wong *et al.* (2022), shows that both methods produced consistent decreases in e_i/e_s with increasing VPD. Thus, our observation that e_i/e_s progressively declines below unity as air VPD increases, as shown in Fig. 2, remains valid.

Differences in the VPD responses of g_s and g_m with and without assuming saturation of e_i

A_n and E are directly measured fluxes and thus cannot be affected by whether saturation or unsaturation is assumed. A_n decreased but E increased with increasing VPD (Fig. 1), both findings that are consistent with previously reported VPD-response patterns conducted at constant temperatures (Dai *et al.*, 1992; Maroco *et al.*, 1997; Yong *et al.*, 1997; Urban *et al.*, 2017). Independent of whether saturation of e_i was assumed, g_s decreased as VPD increased, with a sharper drop in the lower VPD range (Fig. 3). This VPD-response pattern of g_s is consistent with previous findings (Dai *et al.*, 1992; Maroco *et al.*, 1997; Yong *et al.*, 1997; Cernusak *et al.*, 2019). However, the saturation assumption resulted in a considerable underestimation of g_s, and after accounting for unsaturation, the decrease in g_s with increasing VPD became less evident (Fig. 3). These results imply that the impact strength of VPD to induce stomatal closure may have been overestimated in previous studies, which generally assumed saturation of e_i. As a result of the less pronounced VPD response of g_s when unsaturation was accounted for, the intrinsic water use efficiency (i.e. iWUE = A_n/g_s) generally became unresponsive to variations in VPD after accounting for the unsaturation of e_i (Fig. S4).

Both the vapour pressure gradient from the leaf to the air and g_t determine the VPD response of E (Fig. 1b). For the former, e_i/e_s plays a role; the latter represents the influence of g_s, considering that g_b was held constant in our experimental conditions. Following Cernusak *et al.* (2024), the extent to which variations in E as air VPD increased were driven by e_i/e_s and g_s are shown in Fig. S5. For the two species measured at a T_{cuv} of 30°C (*P. abies* and *Q. petraea*), the reduction in potential E reached *c.* −25% due to reduced e_i/e_s and *c.* −46% due to reduced g_t. For the two species measured at a T_{cuv} of 35°C (*F. sylvatica* and *T. cordata*), the reduction in potential E reached *c.* −45% due to reduced e_i/e_s and *c.* −29% due to reduced g_t. These results suggest that both e_i/e_s and g_s make important contributions to driving E in response to increasing air VPD and that their relative importance could depend on temperature.

Accounting for unsaturation had a greater impact on the VPD-response pattern of g_{m13} than on that of g_s. The variable g_{m13} exhibited a shift from no significant response to VPD when e_i was assumed to be saturated (Fig. 4a) to a significant decreasing trend in response to increasing VPD when unsaturation of e_i was considered (Fig. 4b). The result for g_{m13} under unsaturation is in line with findings from some previous studies (Bongi & Loreto, 1989; Loucos *et al.*, 2017; Holloway-Phillips *et al.*, 2019). The decrease in g_m with increasing VPD could be related to decreases in membrane and cell wall permeability and to CO_2 transport by aquaporins (Evans, 2021; Márquez & Busch, 2024).

Differences in the VPD responses of the CO_2 mole fraction inside the leaf with and without assuming saturation of e_i

We found significant decreases in c_i/c_a and c_c/c_a with increasing VPD, both with and without the saturation assumption (Fig. 5). It could be that the combined action of reduced g_s and g_m (Figs 3, 4b) limited the CO_2 supply inside chloroplasts, thus leading to suppressed photosynthesis (Fig. 1a). $\Delta^{13}C_{obs}$ and $\Delta^{18}O_{obs}$ (Fig. S2) were unaffected by whether saturation is assumed, as they were directly derived from the isotope measurements. The decrease in $\Delta^{13}C_{obs}$ with increasing VPD (Fig. S2a) independently supports the results of c_c/c_a, as a decrease in c_c results in decreased $\Delta^{13}C_{obs}$ (Farquhar *et al.*, 1982; Evans *et al.*, 1986). While c_{ca} taking into account unsaturation was calculated from assumed constant g_{m18} values (Eqn 5), c_{ca} assuming saturation was not (Eqn 4). Nevertheless, in both cases, c_{ca}/c_a only slightly decreased with increasing air VPD (Fig. 5b,e), differing from the results for c_i/c_a and c_c/c_a (Fig. 5). The maintained c_{ca}/c_a at high VPD is supported by the increase in $\Delta^{18}O_{obs}$ with increasing VPD (Fig. S2b), indicating continuous CO_2 diffusion into leaves which exchanged O atoms at the sites of carbonic anhydrase activity with leaf water and progressively isotopically enriched as VPD increased (Gillon & Yakir, 2000).

We found that taking unsaturation into account induced a great change in the VPD-response pattern of c_i/c_a (Fig. 5a,d). The saturation assumption leads to an overestimation of the role of VPD in inducing stomatal closure and, consequently, in reducing c_i, as shown here. This would cause biased estimations of other parameters that involve c_i, for example, maximum rates of carboxylation and electron transport, as well as the rate of respiration in the presence of light derived from A_n–c_i curves. While corrections of c_i based on the unsaturation conditions of leaf intercellular spaces are not yet feasible in many cases, care should be taken regarding data interpretation involving c_i derived from conventional leaf gas exchange measurements. Surprisingly, even though a dramatic difference was shown for the estimations of g_{m13} with and without assuming saturation (Fig. 4), the VPD responses of c_c were not so different under the two scenarios (Fig. 5c,f). This result questions the significance of g_m in constraining the diffusion of CO_2 inside leaves, which is in agreement with the rising awareness that g_m and c_c do not necessarily covary (Bahar *et al.*, 2018; Diao *et al.*, 2024).

Implications for leaf water potential and water transport mechanisms

The unsaturation of e_i implies very negative water potentials in the intercellular air spaces and the apoplast (cell walls) (Buckley & Sack, 2019; Rockwell *et al.*, 2022; Scoffoni *et al.*, 2023; Jain *et al.*, 2024). Based on the calculations of Buckley & Sack (2019),

the lowest reported intercellular RH of *c.* 0.7 in our study corresponds to a water potential of *c.* −50 MPa. Given that a 1% decline in intercellular RH reduces water potential by *c.* 1.4 MPa (Buckley & Sack, 2019), very low-water potential values could occur in a range of RH levels. It is difficult to know at which location inside the leaf tissue such extraordinarily negative water potentials would occur, considering that water vapour potentially travels from the evaporation sites deeper into the mesophyll air spaces through the substomatal cavity to reach the stomatal pore (Wong *et al.*, 2022). Nevertheless, a bulk leaf water potential value this negative would be lethal for most plants (Bartlett *et al.*, 2012, 2016; Klein, 2014). However, we did not observe any sign of wilting in any of the tested species throughout the measurements. Therefore, we must assume that: (1) the extreme negative water potential is restricted to the apoplast and (2) the leaf water potential in living cells and bulk leaf water potential are much less negative than that in the apoplast.

These assumptions imply that the plasma membranes would be far less permeable to water at high VPD to sustain such a substantial difference in the water potential between the apoplast and inside the living cells (Wong *et al.*, 2022; Scoffoni *et al.*, 2023; Cernusak *et al.*, 2024). According to the estimation of Wong *et al.* (2022), this permeability is indeed expected to be lower than values reported in previous studies (Morillon & Chrispeels, 2001; Martre *et al.*, 2002). However, as *E* increased with increasing VPD (Fig. 1b), other water flow pathways could be dominant to sustain the water supply to the evaporation surfaces at high VPD. The symplastic pathway through plasmodesmata could be responsible for sustaining water movement between cells, although this is still under debate (Fricke, 2000; Barbour & Farquhar, 2004).

Although the plasma membrane potentially has sharply reduced conductance to water at high VPD, it apparently can largely maintain its conductance for CO_2 transport. In support of this perspective, at the highest VPD, c_c/c_a showed a small reduction when saturation was assumed (Fig. 5c) and a moderate reduction when unsaturation was accounted for (Fig. 5f), compared with c_i/c_a (Fig. 5a,d), suggesting a high plasma membrane conductivity for CO_2 at high VPD. The membrane conductance to CO_2 can be facilitated by some aquaporins (Uehlein *et al.*, 2008; Zhao *et al.*, 2017; Chen *et al.*, 2023). Moreover, it has been hypothesized that the aquaporin-mediated regulation of diffusion can be different for CO_2 and H_2O (Otto *et al.*, 2010; Kaldenhoff, 2012). It has been proposed that aquaporin subunits with different affinities to CO_2 and H_2O compete in the formation of aquaporin complexes, which reduces water permeability when CO_2 conductivity through aquaporins is high (Flexas *et al.*, 2012; Hommel *et al.*, 2014). Certainly, more studies are required to reconcile the mismatch between unsaturation of leaf air spaces and leaf water potential. This has strong implications for improving our understanding of leaf water transport mechanisms and could potentially change our fundamental understanding of leaf CO_2 and H_2O exchange.

Acknowledgements

We acknowledge technical support from the WSL Stable Isotope Research Centre, specifically assistance provided by Manuela Oettli. We are grateful for contributions from Herbert Kurmann, Max Hälg and Walter Godli in setting up the infrastructure. The study was supported by the Swiss National Science Foundation (PZ00P2_179978 and IZCOZ0_205492 granted to MML, as well as 206021_189724 granted to AG and MS) and by WSL Birmensdorf (innovative research grant PPF2020 granted to MML and a visiting fellowship granted to LAC). HD acknowledges funding from the Velux Stiftung (project number 1733). LAC acknowledges funding from the Australian Research Council (project DP210103186).

Competing interests

None declared.

Author contributions

HD, LAC, MML and RTWS conceived the study. MML supervised the project. HD and RTWS set up the instrumentation and carried out the experimental work. HD and LAC processed the experimental data and performed the analysis. HD wrote the manuscript, whilst LAC, MS, AG, RTWS and MML contributed critically to the manuscript.

ORCID

Lucas A. Cernusak https://orcid.org/0000-0002-7575-5526
Haoyu Diao https://orcid.org/0000-0002-8404-1998
Arthur Gessler https://orcid.org/0000-0002-1910-9589
Marco M. Lehmann https://orcid.org/0000-0003-2962-3351
Matthias Saurer https://orcid.org/0000-0002-3954-3534
Rolf T. W. Siegwolf https://orcid.org/0000-0002-0249-0651

Data availability

All data used in this study are available in the Supporting Information Dataset S1.

References

Adnew GA, Pons TL, Koren G, Peters W, Röckmann T. 2020. Leaf-scale quantification of the effect of photosynthetic gas exchange on $\Delta^{17}O$ of atmospheric CO_2. *Biogeosciences* **17**: 3903–3922.

Bahar NHA, Hayes L, Scafaro AP, Atkin OK, Evans JR. 2018. Mesophyll conductance does not contribute to greater photosynthetic rate per unit nitrogen in temperate compared with tropical evergreen wet-forest tree leaves. *New Phytologist* **218**: 492–505.

Barbour MM, Evans JR, Simonin KA, von Caemmerer S. 2016. Online CO_2 and H_2O oxygen isotope fractionation allows estimation of mesophyll conductance in C_4 plants, and reveals that mesophyll conductance decreases as leaves age in both C_4 and C_3 plants. *New Phytologist* **210**: 875–889.

Barbour MM, Farquhar GD. 2004. Do pathways of water movement and leaf anatomical dimensions allow development of gradients in $H_2{}^{18}O$ between veins and the sites of evaporation within leaves? *Plant, Cell & Environment* **27**: 107–121.

Bartlett MK, Klein T, Jansen S, Choat B, Sack L. 2016. The correlations and sequence of plant stomatal, hydraulic, and wilting responses to drought. *Proceedings of the National Academy of Sciences, USA* **113**: 13098–13103.

Bartlett MK, Scoffoni C, Sack L. 2012. The determinants of leaf turgor loss point and prediction of drought tolerance of species and biomes: a global meta-analysis. *Ecology Letters* **15**: 393–405.

Bongi G, Loreto F. 1989. Gas-exchange properties of salt-stressed olive (*Olea europea* L.) leaves. *Plant Physiology* **90**: 1408–1416.

Buckley TN. 2019. How do stomata respond to water status? *New Phytologist* **224**: 21–36.

Buckley TN, Sack L. 2019. The humidity inside leaves and why you should care: implications of unsaturation of leaf intercellular airspaces. *American Journal of Botany* **106**: 618–621.

Busch FA, Holloway-Phillips M, Stuart-Williams H, Farquhar GD. 2020. Revisiting carbon isotope discrimination in C_3 plants shows respiration rules when photosynthesis is low. *Nature Plants* **6**: 245–258.

Busch FA, Sage TL, Cousins AB, Sage RF. 2013. C_3 plants enhance rates of photosynthesis by reassimilating photorespired and respired CO_2. *Plant, Cell & Environment* **36**: 200–212.

von Caemmerer S, Farquhar GD. 1981. Some relationships between the biochemistry of photosynthesis and the gas exchange of leaves. *Planta* **153**: 376–387.

Canny MJ, Huang CX. 2006. Leaf water content and palisade cell size. *New Phytologist* **170**: 75–85.

Cernusak LA, Farquhar GD, Wong SC, Stuart-Williams H. 2004. Measurement and interpretation of the oxygen isotope composition of carbon dioxide respired by leaves in the dark. *Plant Physiology* **136**: 3350–3363.

Cernusak LA, Goldsmith GR, Arend M, Siegwolf RTW. 2019. Effect of vapor pressure deficit on gas exchange in wild-type and abscisic acid-insensitive plants. *Plant Physiology* **181**: 1573–1586.

Cernusak LA, Ubierna N, Jenkins MW, Garrity SR, Rahn T, Powers HH, Hanson DT, Sevanto S, Wong SC, McDowell NG *et al.* 2018. Unsaturation of vapour pressure inside leaves of two conifer species. *Scientific Reports* **8**: 7667.

Cernusak LA, Wong SC, Stuart-Williams H, Márquez DA, Pontarin N, Farquhar GD. 2024. Unsaturation in the air spaces of leaves and its implications. *Plant, Cell & Environment* **2**: 15001.

Chen J, Yue K, Shen L, Zheng C, Zhu Y, Han K, Kai L. 2023. Aquaporins and CO_2 diffusion across biological membrane. *Frontiers in Physiology* **14**: 1205290.

Cousins AB, Mullendore DL, Sonawane BV. 2020. Recent developments in mesophyll conductance in C_3, C_4, and crassulacean acid metabolism plants. *The Plant Journal* **101**: 816–830.

Craig H, Gordon LI. 1965. Deuterium and oxygen-18 variations in the ocean and the marine atmosphere. In: Tongiorgi E, ed. *Proceedings of a conference on stable isotopes in oceanographic studies and palaeotemperatures*. Pisa, Italy: Lischi and Figli, 9–130.

Dai Z, Edwards GE, Ku MSB. 1992. Control of photosynthesis and stomatal conductance in *Ricinus communis* L. (Castor Bean) by leaf to air vapor pressure deficit 1. *Plant Physiology* **99**: 1426–1434.

Devi MJ, Reddy VR. 2018. Transpiration response of cotton to vapor pressure deficit and its relationship with stomatal traits. *Frontiers in Plant Science* **9**: 1572.

Diao H, Cernusak LA, Saurer M, Gessler A, Siegwolf RTW, Lehmann MM. 2024. Uncoupling of stomatal conductance and photosynthesis at high temperatures: mechanistic insights from online stable isotope techniques. *New Phytologist* **241**: 2366–2378.

Duursma RA, Barton CVM, Lin Y-S, Medlyn BE, Eamus D, Tissue DT, Ellsworth DS, McMurtrie RE. 2014. The peaked response of transpiration rate to vapour pressure deficit in field conditions can be explained by the temperature optimum of photosynthesis. *Agricultural and Forest Meteorology* **189-190**: 2–10.

Egorov V, Karpushkin L. 1988. Determination of air humidity over evaporating surface inside a leaf by a compensation method. *Photosynthetica* **22**: 394–404.

Evans J, Sharkey T, Berry J, Farquhar G. 1986. Carbon isotope discrimination measured concurrently with gas exchange to investigate CO_2 diffusion in leaves of higher plants. *Functional Plant Biology* **13**: 281–292.

Evans JR. 2021. Mesophyll conductance: walls, membranes and spatial complexity. *New Phytologist* **229**: 1864–1876.

Fang Z, Zhang W, Brandt M, Abdi AM, Fensholt R. 2022. Globally increasing atmospheric aridity over the 21st century. *Earth's Future* **10**: e2022EF003019.

Farquhar G. 1978. Feedforward responses of stomata to humidity. *Functional Plant Biology* **5**: 787–800.

Farquhar GD, Cernusak LA. 2012. Ternary effects on the gas exchange of isotopologues of carbon dioxide. *Plant, Cell & Environment* **35**: 1221–1231.

Farquhar GD, Lloyd J, Taylor JA, Flanagan LB, Syvertsen JP, Hubick KT, Wong SC, Ehleringer JR. 1993. Vegetation effects on the isotope composition of oxygen in atmospheric CO_2. *Nature* **363**: 439–443.

Farquhar GD, O'Leary MH, Berry JA. 1982. On the relationship between carbon isotope discrimination and the intercellular carbon dioxide concentration in leaves. *Functional Plant Biology* **9**: 121–137.

Farquhar GD, Raschke K. 1978. On the resistance to transpiration of the sites of evaporation within the leaf 1. *Plant Physiology* **61**: 1000–1005.

Flexas J, Barbour MM, Brendel O, Cabrera HM, Carriquí M, Díaz-Espejo A, Douthe C, Dreyer E, Ferrio JP, Gago J *et al.* 2012. Mesophyll diffusion conductance to CO_2: an unappreciated central player in photosynthesis. *Plant Science* **193–194**: 70–84.

Franks PJ, Cowan IR, Farquhar GD. 1997. The apparent feedforward response of stomata to air vapour pressure deficit: information revealed by different experimental procedures with two rainforest trees. *Plant, Cell & Environment* **20**: 142–145.

Fricke W. 2000. Water movement between epidermal cells of barley leaves – a symplastic connection? *Plant, Cell & Environment* **23**: 991–997.

Fu Z, Ciais P, Prentice IC, Gentine P, Makowski D, Bastos A, Luo X, Green JK, Stoy PC, Yang H *et al.* 2022. Atmospheric dryness reduces photosynthesis along a large range of soil water deficits. *Nature Communications* **13**: 989.

Gaastra P. 1959. *Photosynthesis of crop plants as influenced by light, carbon dioxide, temperature, and stomatal diffusion resistance*. Wageningen, the Netherlands: Veenman.

Gillon JS, Yakir D. 2000. Internal conductance to CO_2 diffusion and $C^{18}OO$ discrimination in C_3 leaves. *Plant Physiology* **123**: 201–214.

Goff JA, Gratch S. 1946. Low-pressure properties of water from −160 to 212F. *Transactions of the American Society of Heating and Ventilating Engineers* **52**: 95–122.

Grossiord C, Buckley TN, Cernusak LA, Novick KA, Poulter B, Siegwolf RTW, Sperry JS, McDowell NG. 2020. Plant responses to rising vapor pressure deficit. *New Phytologist* **226**: 1550–1566.

Hochberg U, Rockwell FE, Holbrook NM, Cochard H. 2018. Iso/Anisohydry: a plant–environment interaction rather than a simple hydraulic trait. *Trends in Plant Science* **23**: 112–120.

Holloway-Phillips M, Cernusak LA, Stuart-Williams H, Ubierna N, Farquhar GD. 2019. Two-source $\delta^{18}O$ method to validate the $CO^{18}O$-photosynthetic discrimination model: implications for mesophyll conductance. *Plant Physiology* **181**: 1175–1190.

Hommel R, Siegwolf R, Saurer M, Farquhar GD, Kayler Z, Ferrio JP, Gessler A. 2014. Drought response of mesophyll conductance in forest understory species – impacts on water-use efficiency and interactions with leaf water movement. *Physiologia Plantarum* **152**: 98–114.

IPCC. 2021. Climate change 2021: the physical science basis. In: Masson-Delmotte V, Zhai P, Pirani A, Connors SL, Péan C, Berger S, Caud N, Chen Y, Goldfarb L, Gomis MI *et al.*, eds. *Contribution of Working Group I to the Sixth Assessment Report of the Intergovernmental Panel on Climate Change*. Cambridge, UK and New York, NY, USA: Cambridge University Press.

Jain P, Huber AE, Rockwell FE, Sen S, Holbrook NM, Stroock AD. 2024. New approaches to dissect leaf hydraulics reveal large gradients in living tissues of tomato leaves. *New Phytologist* **242**: 453–465.

Jarvis PG, Slatyer RO. 1970. The role of the mesophyll cell wall in leaf transpiration. *Planta* **90**: 303–322.

Jones HG, Higgs KH. 1980. Resistance to water loss from the mesophyll cell surface in plant leaves. *Journal of Experimental Botany* **31**: 545–553.

Kaldenhoff R. 2012. Mechanisms underlying CO_2 diffusion in leaves. *Current Opinion in Plant Biology* **15**: 276–281.

Karpushkin L. 1994. A compensation gasometric method for estimating the kinetic parameters of H_2O and CO_2 exchange in plant leaves. *Russian Journal of Plant Physiology* **41**: 410–413.

Klein T. 2014. The variability of stomatal sensitivity to leaf water potential across tree species indicates a continuum between isohydric and anisohydric behaviours. *Functional Ecology* **28**: 1313–1320.

Kuznetsova A, Brockhoff PB, Christensen RHB. 2017. LMERTEST package: tests in linear mixed effects models. *Journal of Statistical Software* **82**: 1–26.

Loucos KE, Simonin KA, Barbour MM. 2017. Leaf hydraulic conductance and mesophyll conductance are not closely related within a single species. *Plant, Cell & Environment* **40**: 203–215.

Maroco J, Atilde PO, Pereira J, Atilde SO, Chaves MM. 1997. Stomatal responses to leaf-to-air vapour pressure deficit in Sahelian species. *Functional Plant Biology* **24**: 381–387.

Márquez DA, Busch FA. 2024. The interplay of short-term mesophyll and stomatal conductance responses under variable environmental conditions. *Plant, Cell & Environment* **2**: 1–18.

Márquez DA, Stuart-Williams H, Cernusak LA, Farquhar GD. 2023. Assessing the CO_2 concentration at the surface of photosynthetic mesophyll cells. *New Phytologist* **238**: 1446–1460.

Martre P, Morillon R, Barrieu FO, North GB, Nobel PS, Chrispeels MJ. 2002. Plasma membrane aquaporins play a significant role during recovery from water deficit. *Plant Physiology* **130**: 2101–2110.

McDowell NG, Sapes G, Pivovaroff A, Adams HD, Allen CD, Anderegg WRL, Arend M, Breshears DD, Brodribb T, Choat B *et al.* 2022. Mechanisms of woody-plant mortality under rising drought, CO_2 and vapour pressure deficit. *Nature Reviews Earth and Environment* **3**: 294–308.

Morillon R, Chrispeels MJ. 2001. The role of ABA and the transpiration stream in the regulation of the osmotic water permeability of leaf cells. *Proceedings of the National Academy of Sciences, USA* **98**: 14138–14143.

Moss DN, Rawlins SL. 1963. Concentration of carbon dioxide inside leaves. *Nature* **197**: 1320–1321.

Novick KA, Ficklin DL, Grossiord C, Konings AG, Martínez-Vilalta J, Sadok W, Trugman AT, Williams AP, Wright AJ, Abatzoglou JT *et al.* 2024. The impacts of rising vapour pressure deficit in natural and managed ecosystems. *Plant, Cell & Environment* **20**: 1–29.

Oren R, Sperry JS, Katul GG, Pataki DE, Ewers BE, Phillips N, Schäfer KVR. 1999. Survey and synthesis of intra- and interspecific variation in stomatal sensitivity to vapour pressure deficit. *Plant, Cell & Environment* **22**: 1515–1526.

Otto B, Uehlein N, Sdorra S, Fischer M, Ayaz M, Belastegui-Macadam X, Heckwolf M, Lachnit M, Pede N, Priem N *et al.* 2010. Aquaporin tetramer composition modifies the function of tobacco aquaporins. *Journal of Biological Chemistry* **285**: 31253–31260.

Peak D, Mott KA. 2011. A new, vapour-phase mechanism for stomatal responses to humidity and temperature. *Plant, Cell & Environment* **34**: 162–178.

Perez-Martin A, Flexas J, Ribas-Carbó M, Bota J, Tomás M, Infante JM, Diaz-Espejo A. 2009. Interactive effects of soil water deficit and air vapour pressure deficit on mesophyll conductance to CO_2 in *Vitis vinifera* and *Olea europaea*. *Journal of Experimental Botany* **60**: 2391–2405.

R Core Team. 2023. *R: a language and environment for statistical computing.* Vienna, Austria: R Foundation for Statistical Computing.

Rockwell FE, Holbrook NM, Jain P, Huber AE, Sen S, Stroock AD. 2022. Extreme undersaturation in the intercellular airspace of leaves: a failure of Gaastra or Ohm? *Annals of Botany* **130**: 301–316.

Schönbeck LC, Schuler P, Lehmann MM, Mas E, Mekarni L, Pivovaroff AL, Turberg P, Grossiord C. 2022. Increasing temperature and vapour pressure deficit lead to hydraulic damages in the absence of soil drought. *Plant, Cell & Environment* **45**: 3275–3289.

Scoffoni C, Albuquerque C, Buckley TN, Sack L. 2023. The dynamic multi-functionality of leaf water transport outside the xylem. *New Phytologist* **239**: 2099–2107.

Sharkey TD, Imai K, Farquhar GD, Cowan IR. 1982. A direct confirmation of the standard method of estimating intercellular partial pressure of CO_2. *Plant Physiology* **69**: 657–659.

Shekhar A, Hörtnagl L, Buchmann N, Gharun M. 2023. Long-term changes in forest response to extreme atmospheric dryness. *Global Change Biology* **29**: 5379–5396.

Shirke PA, Pathre UV. 2004. Influence of leaf-to-air vapour pressure deficit (VPD) on the biochemistry and physiology of photosynthesis in *Prosopis juliflora*. *Journal of Experimental Botany* **55**: 2111–2120.

Smith MN, Taylor TC, van Haren J, Rosolem R, Restrepo-Coupe N, Adams J, Wu J, de Oliveira RC, da Silva R, de Araujo AC *et al.* 2020. Empirical evidence for resilience of tropical forest photosynthesis in a warmer world. *Nature Plants* **6**: 1225–1230.

Stangl ZR, Tarvainen L, Wallin G, Marshall JD. 2022. Limits to photosynthesis: seasonal shifts in supply and demand for CO_2 in Scots pine. *New Phytologist* **233**: 1108–1120.

Stangl ZR, Tarvainen L, Wallin G, Ubierna N, Räntfors M, Marshall JD. 2019. Diurnal variation in mesophyll conductance and its influence on modelled water-use efficiency in a mature boreal *Pinus sylvestris* stand. *Photosynthesis Research* **141**: 53–63.

Trotsiuk V, Babst F, Grossiord C, Gessler A, Forrester DI, Buchmann N, Schaub M, Eugster W. 2021. Tree growth in Switzerland is increasingly constrained by rising evaporative demand. *Journal of Ecology* **109**: 2981–2990.

Uehlein N, Otto B, Hanson DT, Fischer M, McDowell N, Kaldenhoff R. 2008. Function of *Nicotiana tabacum* aquaporins as chloroplast gas pores challenges the concept of membrane CO_2 permeability. *Plant Cell* **20**: 648–657.

Urban J, Ingwers MW, McGuire MA, Teskey RO. 2017. Increase in leaf temperature opens stomata and decouples net photosynthesis from stomatal conductance in *Pinus taeda* and *Populus deltoides x nigra*. *Journal of Experimental Botany* **68**: 1757–1767.

Ward DA, Bunce JA. 1986. Novel evidence for a lack of water vapour saturation within the intercellular airspace of turgid leaves of mesophytic species. *Journal of Experimental Botany* **37**: 504–516.

Warren CR. 2008. Soil water deficits decrease the internal conductance to CO_2 transfer but atmospheric water deficits do not. *Journal of Experimental Botany* **59**: 327–334.

Wingate L, Seibt U, Moncrieff JB, Jarvis PG, Lloyd J. 2007. Variations in ^{13}C discrimination during CO_2 exchange by *Picea sitchensis* branches in the field. *Plant, Cell & Environment* **30**: 600–616.

Wong SC, Canny MJ, Holloway-Phillips M, Stuart-Williams H, Cernusak LA, Márquez DA, Farquhar GD. 2022. Humidity gradients in the air spaces of leaves. *Nature Plants* **8**: 971–978.

Yong JWH, Wong SC, Farquhar GD. 1997. Stomatal responses to changes in vapour pressure difference between leaf and air. *Plant, Cell & Environment* **20**: 1213–1216.

Yuan W, Zheng Y, Piao S, Ciais P, Lombardozzi D, Wang Y, Ryu Y, Chen G, Dong W, Hu Z *et al.* 2019. Increased atmospheric vapor pressure deficit reduces global vegetation growth. *Science Advances* **5**: eaax1396.

Zhao M, Tan H-T, Scharwies J, Levin K, Evans JR, Tyerman SD. 2017. Association between water and carbon dioxide transport in leaf plasma membranes: assessing the role of aquaporins. *Plant, Cell & Environment* **40**: 789–801.

Zweifel R, Sterck F, Braun S, Buchmann N, Eugster W, Gessler A, Häni M, Peters RL, Walthert L, Wilhelm M *et al.* 2021. Why trees grow at night. *New Phytologist* **231**: 2174–2185.

Supporting Information

Additional Supporting Information may be found online in the Supporting Information section at the end of the article.

Dataset S1 The dataset analysed in this study.

Fig. S1 Variations in air relative humidity (RH) with increasing air vapour pressure deficit (VPD).

Fig. S2 Online stable carbon ($\Delta^{13}C_{obs}$) and oxygen ($\Delta^{18}O_{obs}$) discriminations of CO_2 during assimilation in response to increasing air vapour pressure deficit (VPD).

Fig. S3 Response of leaf intercellular relative humidity (e_i/e_s) to increasing air vapour pressure deficit (VPD).

Fig. S4 Responses of intrinsic water use efficiency (iWUE) to increasing air vapour pressure deficit (VPD).

Fig. S5 Impacts of leaf intercellular relative humidity (e_i/e_s) and leaf conductance (g_t) on the potential transpiration rate (E) with increasing air vapour pressure deficit (VPD).

Methods S1 Supplementary equations for calculations of intercellular relative humidity from $\delta^{18}O$.

Please note: Wiley is not responsible for the content or functionality of any Supporting Information supplied by the authors. Any queries (other than missing material) should be directed to the *New Phytologist* Central Office.